Resource

Multifaceted atlases of the human brain in its infancy

Sahar Ahmad , **Ye Wu** , **Zhengwang Wu, Kim-Han Thung, Siyuan Liu** , **Weili Lin, Gang Li** , **Li Wang** & **Pew-Thian Yap** ✉

Brain atlases are spatial references for integrating, processing, and analyzing brain features gathered from different individuals, sources, and scales. Here we introduce a collection of joint surface–volume atlases that chart postnatal development of the human brain in a spatiotemporally dense manner from two weeks to two years of age. Our month-specific atlases chart normative patterns and capture key traits of early brain development and are therefore conducive to identifying aberrations from normal developmental trajectories. These atlases will enhance our understanding of early structural and functional development by facilitating the mapping of diverse features of the infant brain to a common reference frame for precise multifaceted quantification of cortical and subcortical changes.

Human brain development is a complex and protracted process that begins during the third gestational week and extends through adulthood[1]. Throughout the late prenatal period and early infancy, the human brain undergoes a myriad of cellular processes, including neurogenesis, neuronal migration, astrogliogenesis, oligodendrogenesis, synaptogenesis, myelination, and synaptic pruning[2] (Supplementary Fig. 1). These cellular events drive the rapid growth of the infant brain during the first two years of life, resulting in structural changes and reorganization of neural circuits[3]. The intracranial volume of the newborn brain doubles during the first postnatal year, attaining approximately 65% of the adult brain volume[4]. The gray matter (GM) volume increases more (~71%) than the white matter (WM) volume (~20%) in the first year. A precise quantification of early brain growth will be conducive to a step change in our understanding of developments that lead to maturation of cognitive functions[3]. However, endeavors in this direction have so far been hindered by the dearth of brain atlases for mapping features of early brain development to common spaces necessary for fine-grained spatiotemporal quantification of brain changes.

Unlike the long-established growth charts utilized by pediatricians to quantify year-to-year maturation in terms of a child's height, weight, and head circumference in relation to standardized curves derived from healthy growing children[5], normative references for neurodevelopment are virtually nonexistent. Recent efforts have been dedicated toward constructing brain charts that capture normative patterns of cerebral development[4] in terms of volumetric growth of GM, WM, and cerebrospinal fluid (CSF), and cortical growth captured by surface area and cortical thickness[6]. Although these brain charts standardize brain morphological measurements, they do not define a common coordinate system for mapping brain features, particularly from multiple imaging modalities, to a unified reference space. An additional limitation of existing brain charts is that they rely on the demarcation of the brain into adjoint but separate brain areas with hypothetically uniform functions, while in reality an extensive body of evidence suggests a more gradual transition of areal boundaries, particularly in association cortices[7]. These limitations call for the construction of atlases that offer standardized coordinate frameworks for concurrent analysis of multimodal data at multiple levels of granularity.

Existing atlases of the baby brain are typically limited to specific prenatal or postnatal periods[8–12] (Supplementary Fig. 2 and Supplementary Table 1). Brain atlases densely covering the entirety of the first two years of life are lacking owing to challenges in collecting longitudinal brain magnetic resonance imaging (MRI) data. Adding to the difficulties in constructing these much-needed atlases are the rapid changes in the sizes and shapes of cerebral structures (Supplementary Fig. 3), and the evolving and often insufficient tissue contrast between WM and GM[13]. Moreover, existing cortical surface and volumetric atlases are typically constructed independently, resulting in the following problems:

Department of Radiology and Biomedical Research Imaging Center, University of North Carolina, Chapel Hill, NC, USA. ✉e-mail: ptyap@med.unc.edu

(i)   misalignment between tissue interfaces of the volumetric atlas and the white and pial surfaces of the cortical atlas;
(ii) fuzzy cortical structures, as volumetric displacements are estimated without taking into account the complex convolutions of the cortical surface;
(iii) anatomically implausible displacements owing to cortical surface registration that is based only on surface attributes but ignoring the volumetric data[14];
(iv) volumetric and cortical surface attributes are not defined in the same space, making it difficult to analyze the two entities concurrently and consistently[15]; and
(v)   diminishing of real but subtle changes owing to inconsistent and inaccurate alignment[16].

In this work, we present a set of month-specific surface–volume longitudinal brain atlases of infants from 2 weeks to 24 months of age. These atlases facilitate the precise mapping of fine-grained changes in both space and time, and are therefore a valuable resource for studying postnatal human brain development, identifying early roots of neurological disorders, and quantifying development-related malformations. We demonstrate that our high-fidelity atlases capture the normative evolutionary landscape of cortical surface features and tissue volumetric characteristics of the infant brain during the first two years of brain development.

Results

Surface–volume consistency
Our atlases allow multifaceted analyses of volumetric and surface data in a common space. As a reference, we first construct the infant brain atlas (IBA) at 12 months, for volume (IBA12-V) and surface (IBA12-S), in a surface–volume consistent manner[17] using high-quality magnetic resonance (MR) images of 37 infant subjects scanned around 12 months of age as part of the Baby Connectome Project (BCP)[18]. The cortical surface and volumetric data of these subjects are simultaneously normalized in space[19] and then fused to form

(i)   the white and pial cortical surfaces of IBA12-S and
(ii) the T1-weighted (T1w) intensity image, T2-weighted (T2w) intensity image, and the WM, GM, and CSF tissue maps of IBA12-V.

In contrast to atlases constructed with Spherical Demons[20] and ANTs[21], IBA12-V, and IBA12-S exhibit sharp anatomical details despite being an average of a few tens of subjects (Fig. 1), thanks to the alignment of GM–WM boundaries via explicit registration of cortical surfaces. In fact, IBA12-V resembles MR images of one-year-olds with substantially less fuzziness than the atlas constructed with ANTs without leveraging the geometry of cortical surfaces. This is evident from the close-ups of the temporal and parietal lobes (Fig. 1a,b). Subcortical structures, including the thalamus, caudate nucleus, and putamen, are well defined, indicating that the surface–volume consistent atlas construction process is conducive to preserving both cortical and subcortical anatomical details. While the T1w IBA12-V exhibits adult-like contrast, the T2w IBA12-V is close to isointense with substantial overlap in intensity distributions between WM and GM, consistent with T2w images of one-year-olds[22]. This is particularly noticeable at the superior frontal and rostral middle frontal cortices (Fig. 1b).

The white and pial cortical surfaces of IBA12-S are consistently aligned with the GM–WM and WM–CSF interfaces as delineated by the tissue segmentation maps of IBA12-V (Fig. 1c). This is confirmed by the zoomed-in views of, for example, the lateral occipital, inferior parietal, cuneus, precuneus, medial orbitofrontal, and superior parietal cortices. On the other hand, the ANTs atlas shows inconsistent alignment of the cortical surfaces with tissue interfaces in the volumetric space.

The cortical surfaces of both hemispheres in IBA12-S preserve cortical convolutions with distinct gyral and sulcal patterns (Fig. 1d,e).

For greater clarity, we map the average convexity and mean curvature of the white surface onto a sphere. Mapping is only performed for IBA12-S and ANTs as Spherical Demons outputs only spherical atlases of cortical features. Average convexity captures coarse-scale geometric features of primary sulcal folds[23], whereas mean curvature captures fine-scale geometric features of secondary and tertiary folds. The average convexity maps of the Spherical Demons and IBA12-S atlases are consistent with that of an individual subject. On the other hand, the average convexity map of the ANTs atlas indicates atypical narrowing of the gyral and sulcal folds. Only IBA12-S exhibits typical mean curvature patterns. Spherical Demons gives a fuzzy mean curvature map that fails to capture fine-grained details of cortical folds. ANTs gives an atypical mean curvature map, indicating alteration of surface topology. These results indicate that primary gyri and sulci, including the precentral and postcentral gyri and sulci and the central sulcus, are captured by all three atlases, but localized gyral and sulcal details are only preserved in IBA12-S.

Surface atlases across infancy
Early brain development is characterized by dynamic changes in cortical folding patterns. We constructed month-specific cortical atlases for the first two years of life by longitudinally warping IBA12-S. Major cortical folds of white surfaces—including the central sulcus, precentral and postcentral gyri, inferior parietal lobule, temporal gyrus, superior and inferior temporal sulci, superior frontal gyrus, cingulate gyrus and sulcus, and parieto-occipital sulcus—are consistent across time points (Fig. 2a and Extended Data Figs. 1–3). Mean curvature mapped onto the inflated white surface atlases indicates subtle developments of secondary and tertiary gyri and sulci (Fig. 2b). Cortical thickness measured between the white and pial cortical surfaces of the atlases, projected onto the inflated white surface atlas (Fig. 2c), indicates that the cortical thickness of the prefrontal cortex, temporal lobe, and insula increases. By contrast, the thickness of the visual and sensorimotor cortices increases at a slower pace.

Volumetric atlases across infancy
We generated IBA-V, T1w and T2w atlases from infants 2 weeks to 24 months of age (Fig. 3a,b and Extended Data Figs. 4 and 5). The image contrast evolves month-to-month during year one and becomes adult-like in year two. The T1w and T2w atlases are isointense around 3–6 months and 9–12 months, respectively. The atlases preserve distinct boundaries at the GM–WM interface as evident from the close-ups of the precuneus, cuneus, and inferior parietal cortex (Fig. 3a,b).

Age-specific white and pial cortical surface atlases overlapped on the tissue segmentation atlases (Fig. 3c and Extended Data Fig. 6) indicate that the cortical surface atlases are well aligned with the tissue boundaries of the volumetric atlases, particularly at the superior and middle frontal gyri of both the hemispheres, supramarginal gyrus, inferior parietal cortex, insula, and precentral and postcentral gyri. Good alignment is confirmed by zoomed-in views of the atlases at selected time points (Fig. 3c).

Surface and volumetric development
The IBA captures the developmental features (Supplementary Fig. 4) of typically developing infants in the first two years of life. Compared with the atlases constructed with Spherical Demons and ANTs, the IBA more faithfully reflects the individuals, as evidenced by the smaller mean absolute error between the growth curve for each surface or volumetric feature of the IBA and the population curve obtained by fitting the generalized additive mixture model (GAMM)[24] (Fig. 4a).

We studied the surface and volumetric features captured by the IBA (Fig. 4b,c). During the first and second postnatal years, the IBA-S increases in cortical thickness by 25.7% and 4.3%, increases in surface area by 56.1% and 8.5%, increases in average convexity by 25.5% and 3.6%, and decreases in mean curvature by 20.9% and 3.9% (growth rates are
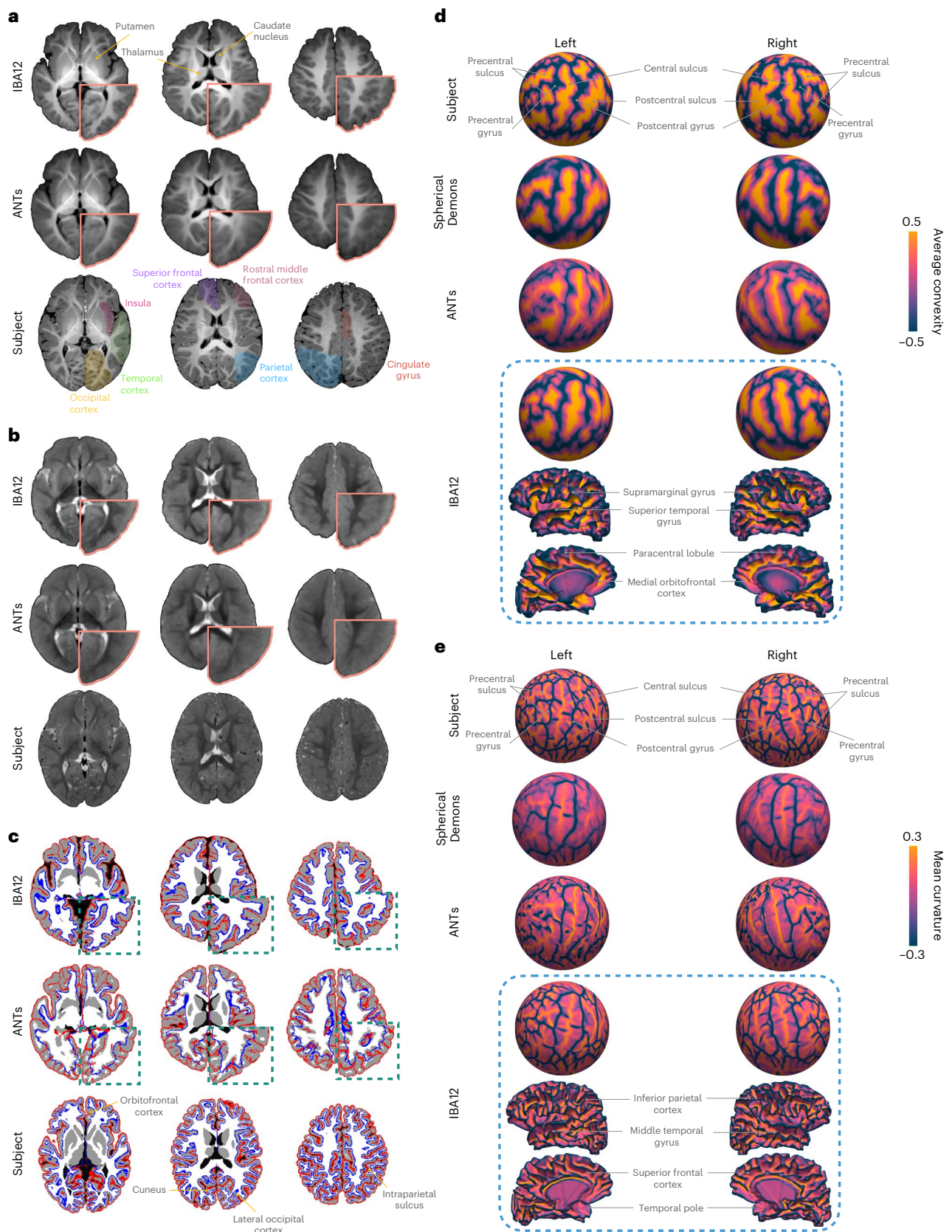
Fig. 1 | The reference infant brain atlas at 12 months. a,b, Transverse sections of T1w and T2w atlases and the T1w and T2w images of an individual subject. **c,** White and pial cortical surface atlases overlaid onto the corresponding tissue segmentation atlases. The cortical surfaces of the individual subject are overlaid onto its tissue segmentation map. **d,** Subject and atlas average convexity maps projected onto a sphere. Lateral and medial views of the IBA12-S white surface colored by average convexity are shown for reference. **e,** Subject and atlas mean curvature maps projected onto a sphere. Lateral and medial views of the IBA12-S white surface colored by mean curvature are shown for reference.

Fig. 2 | Longitudinal white surface atlases of the infant brain. a, Lateral and medial views of white surface atlases from 2 weeks to 24 months, colored by average convexity (mm). **b**, Inflated white surface atlases colored by mean curvature (mm⁻¹). **c**, Inflated white surface atlases colored by cortical thickness (mm).

reported in terms of percentage change). During the same period, the IBA-V increases in GM volume by 97.2% and 13.8%, increases in WM volume by 92.9% and 15.9%, increases in ventricular CSF volume by 89.8% and 10.5%, and increases in whole-brain volume (WBV = GM + WM) by 95.6% and 14.6%. We also report the velocity curves along with peak growth ages, indicating maximal growth rates, for these surface and volumetric features (Supplementary Fig. 5).

Regional analysis indicates spatially heterogeneous development. We measured the thickness of 34 cortical regions-of-interest (ROIs) delineated via FreeSurfer using the Desikan–Killiany atlas[25] (Supplementary Fig. 6). Developmental trajectories of regional cortical thickness show that the insula, frontal cortex, and superior, middle, and inferior temporal cortices are consistently thicker during infancy (Fig. 5). On the other hand, the precentral and postcentral gyri, occipital and inferior parietal cortices, and banks of superior temporal sulcus are thinner throughout the study period. Regional growth rates vary from 21.2% to 32.0% and 2.3% to 6.7% for the first and second postnatal years (Extended Data Fig. 7). The growth rates

(Year 1, Year 2) are (22.6%, 2.3%) for the primary visual cortex, (25.1%, 3.3%) for the primary somatosensory cortex, (24.5%, 4.3%) for the primary motor cortex, (29.5%, 4.0%) for the primary auditory cortex, (27.7%, 4.4%) for the temporal association cortex, (27.6%, 4.4%) for the parietal association cortex, and (23.9%, 4.8%) for the prefrontal association cortex (Extended Data Fig. 7a).

We show the developmental trajectories of regional surface area in Extended Data Fig. 8 and growth rates for the first and second postnatal years in Extended Data Fig. 9. High-expansion regions include rostral anterior cingulate gyrus, medial orbitofrontal gyrus, superior frontal gyrus, rostral middle frontal gyrus, inferior and middle temporal gyri, and superior and inferior parietal gyri. Low-expansion regions include insula, pericalcarine, cuneus, entorhinal, temporal pole, and parahippocampal gyrus. Regional growth rates vary from 20.5% to 49.7% in year 1 and 2.9% to 11.1% in year 2. The growth rates (Year 1, Year 2) are (42.4%, 3.4%) for the primary visual cortex, (36.0%, 5.6%) for the primary somatosensory cortex, (34.1%, 6.0%) for the primary motor cortex, (42.3%, 5.3%) for the primary auditory cortex, (39.8%, 6.9%) for
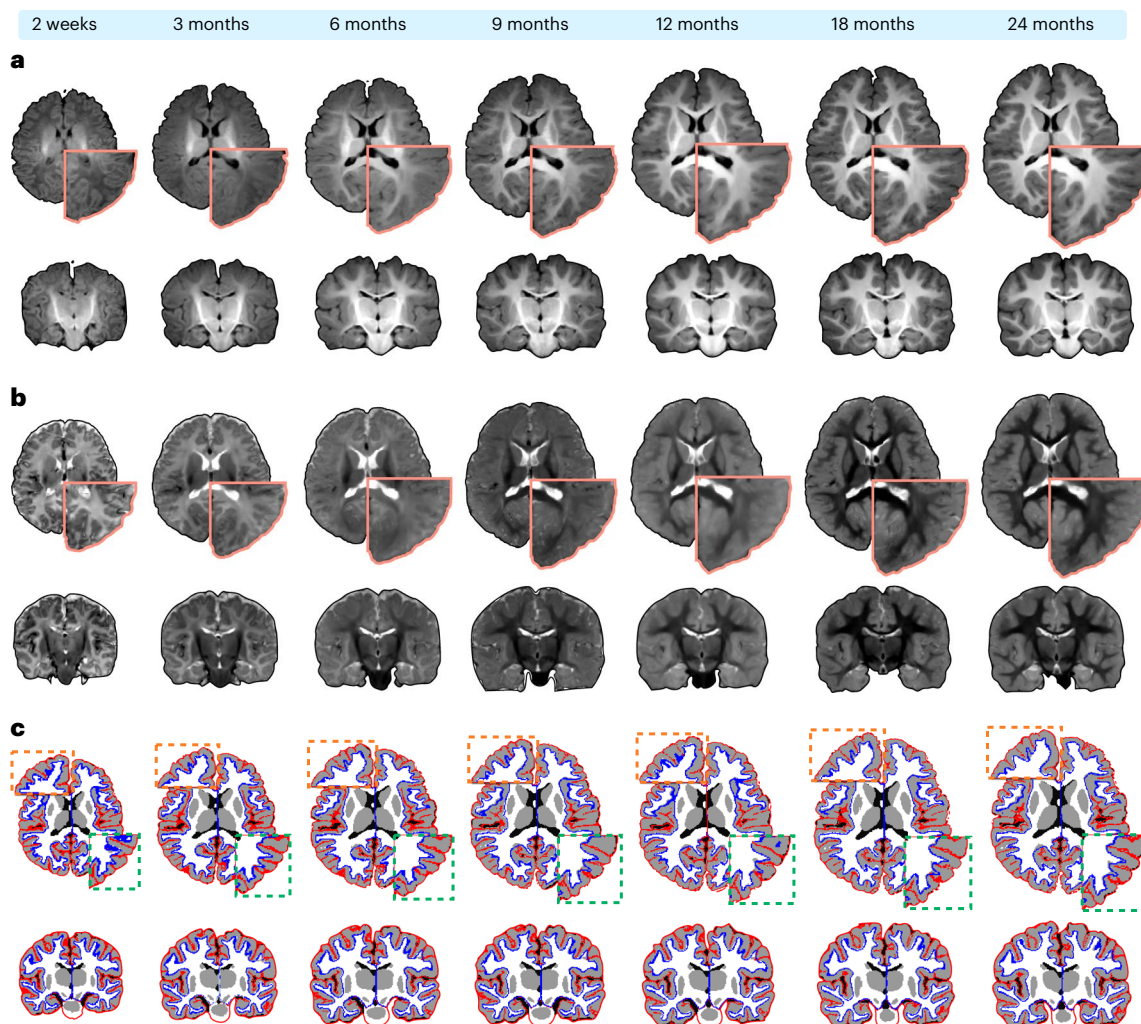
Fig. 3 | Volumetric atlases of the infant brain. a,b, Transverse and coronal sections of the T1w and T2w atlases from 2 weeks to 24 months. **c,** White (*blue*) and pial (*red*) surface atlases overlaid onto the corresponding tissue segmentation atlases.

the temporal association cortex, (38.9%, 5.8%) for the parietal association cortex, and (38.1%, 7.7%) for the prefrontal association cortex (Extended Data Fig. 9a).

The IBA captures the asymmetry of cortical features. We show the hemispheric lateralization of regional cortical features via the laterality index, LI = (left − right)/(left + right), computed for each ROI. There is significant asymmetry (two-tailed t-test; $P < 0.01$) in cortical thickness (Extended Data Fig. 10) and surface area (Supplementary Fig. 7) for majority of the ROIs. The corresponding P values, t-scores, and degrees of freedom are reported for cortical thickness in the source data of Extended Data Fig. 10 and for surface area in Supplementary Data File 2. The ROI-specific mean LI for cortical thickness and surface area are shown in Extended Data Figs. 7b, 9b. Results for other attributes are presented in Supplementary Note 1.

Cortical T1w/T2w ratio
We investigated cortical myelination across infancy by T1w/T2w ratio mapping of the cortical ribbon to the white surface of each individual subject[26]. The GAMM-fitted myelin maps (Fig. 6) indicate increasing myelination in both cerebral hemispheres at average rates of 57.7% and 7.9% in the first and second postnatal years, respectively. Myelination is spatially heterogeneous with heavy myelination in the primary visual, motor, and somatosensory cortices and light myelination in the prefrontal, parietal, and temporal association cortices.

Discussion
Charting normative structural and functional changes during early brain development is key to understanding aberrations associated with neurodevelopmental disorders such as attention-deficit/hyperactivity disorder, dyslexia, and cerebral palsy[27–29]. We have presented a set of longitudinal, unified surface–volume atlases of the infant brain covering every month of the first two postnatal years. These atlases represent a resource that will facilitate the joint investigation of changes in cortical geometries and brain tissues during a period of rapid and critical brain development. Our atlases are substantially better in preserving anatomical details and surface geometric features than ANTs[21,30] and Spherical Demons[20,31].

The human brain undergoes complex gyrification that begins after mid-gestation[32], nudging the initially smooth cerebral surface into a highly convoluted structure. A widely used macroscopic morphological measure is cortical thickness, which is systematically related to the cytoarchitecture and hierarchical structural organization of the cortex[33]. The neurobiological mechanisms underlying developmental changes in cortical thickness are complex and involve processes such as synaptogenesis, proliferation of dendrites and dendritic spines, axonal sprouting, and vascular development[34]. The IBA shows that cortical thickness increases rapidly during the first year and more slowly in the second year. Greater cortical thickness during early brain development is in general positively associated with intelligence and cognitive skills
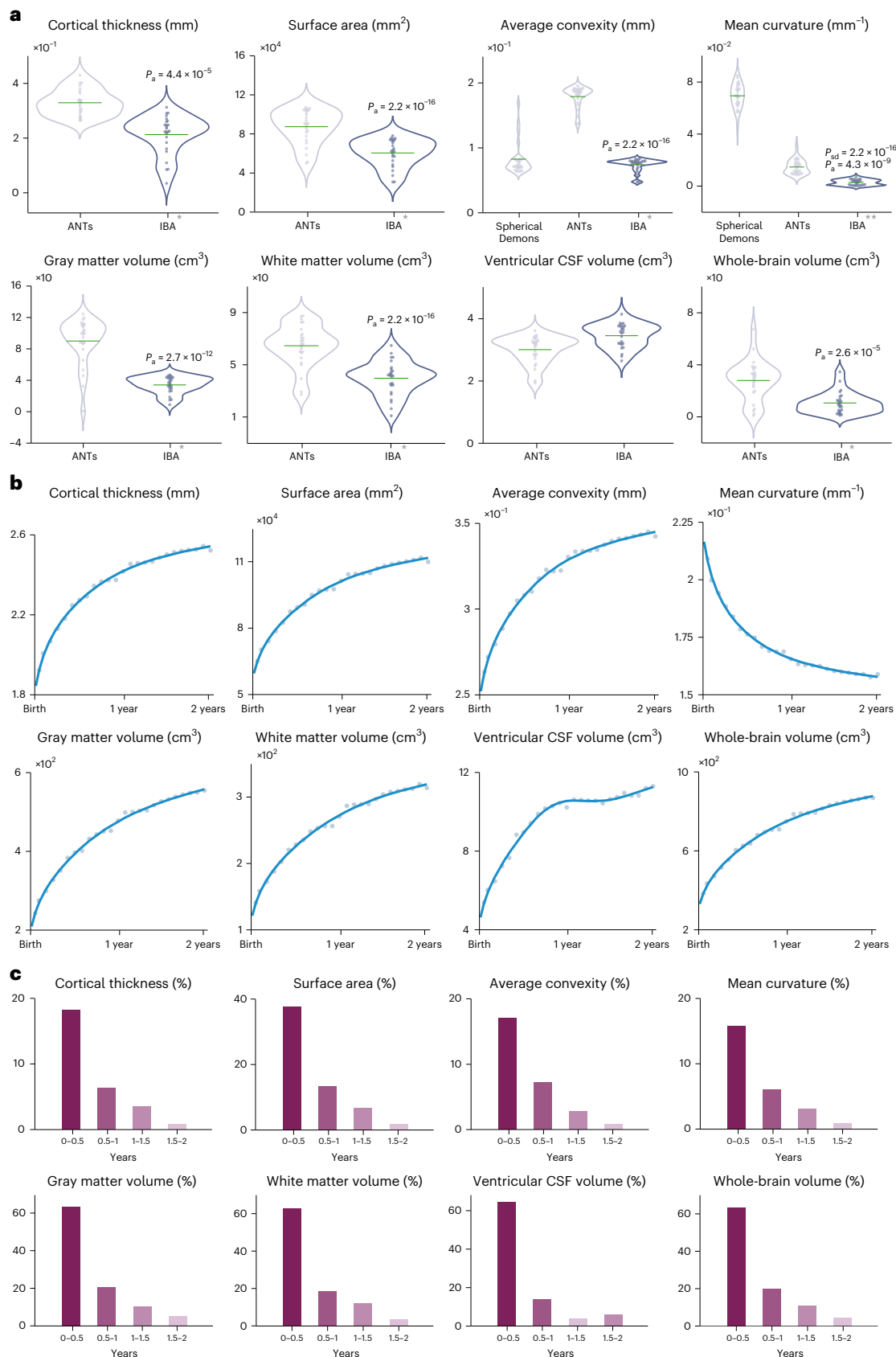
Fig. 4 | Development of surface and volume. a, Violin plots for absolute error of the developmental trajectories of surface and volumetric features, computed between the atlases and the individual subjects. The mean absolute error is marked by a green crossbar. A single star indicates that the mean error for the IBA is significantly different from ANTs (two-tailed paired t-test, P_a). A double star indicates that the mean error for the IBA is significantly different from both Spherical Demons (two-tailed paired t-test, P_{sd}) and ANTs (two-tailed paired t-test, P_a). **b**, Developmental trajectories (adjusted $R^2 = 0.99$) of white surface features and tissue volumes of the IBA. **c**, Surface and volumetric changes every six months.
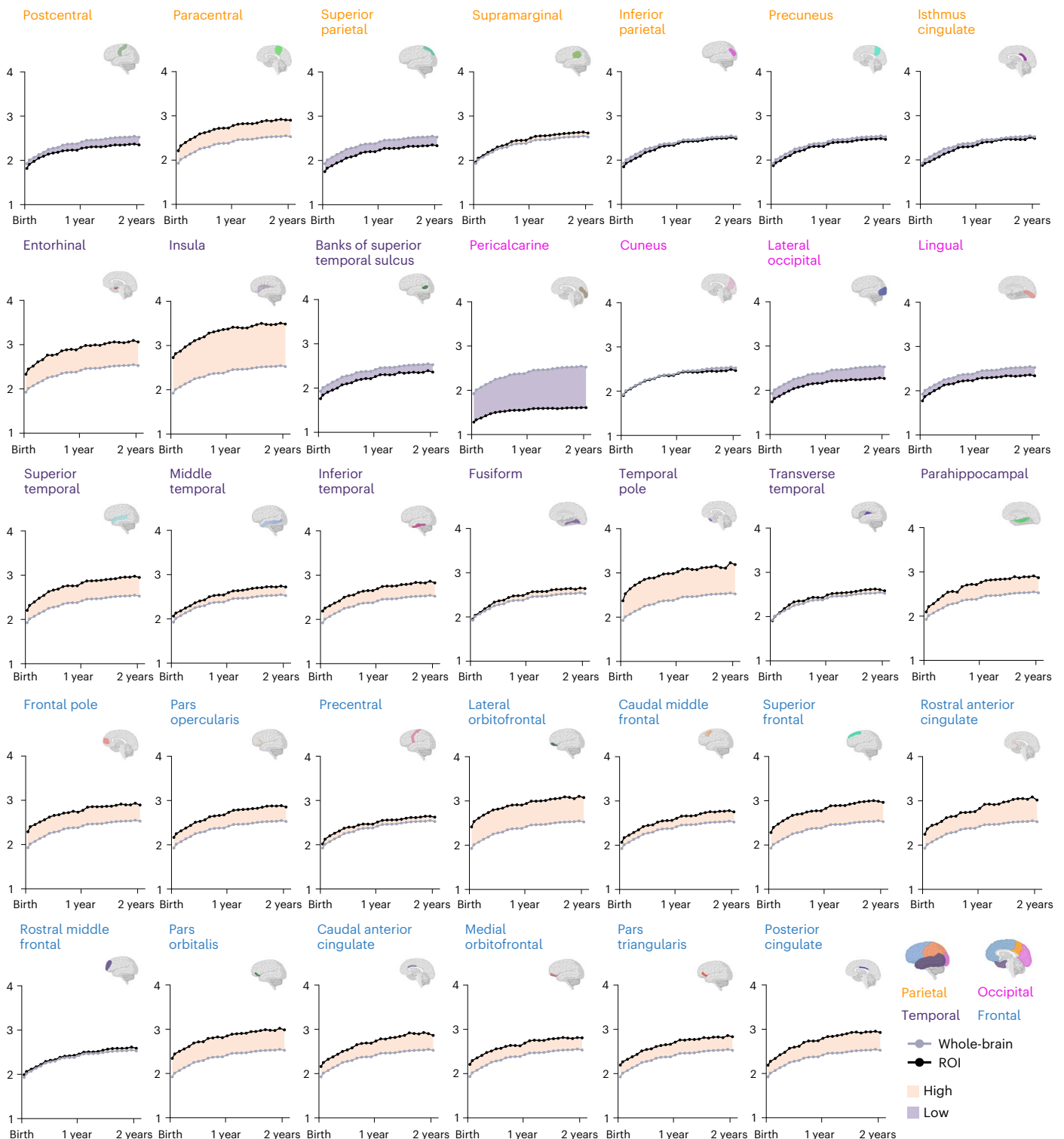
Fig. 5 | Regional developmental trajectories of cortical thickness. Growth curves of cortical thickness for the IBA cortical regions. Shaded regions indicate whether cortical thickness is higher or lower than the whole-brain average.

in later stages of life[35]. The IBA also indicates that cortical thickness changes heterogeneously across the cortex, in line with previous studies[36]. The association cortices in the temporal, parietal, and prefrontal lobes are thicker compared with the primary visual and sensorimotor cortices, which agrees with the fact that thicker cortices are in general less mature. This is consistent with the functional development of the infant brain where vision, motor, and sensory systems are more mature

than executive functions. More discussion on the cortical attributes of the IBA is included in Supplementary Note 2.

In addition to folding geometry, we quantitatively assessed brain tissue volume changes during infancy. Early neurodevelopment is underpinned by cellular and molecular processes that drive the growth and maturation of brain tissues. Cell bodies, axon terminal branches, dendrites, and spines residing in GM contribute to the early growth
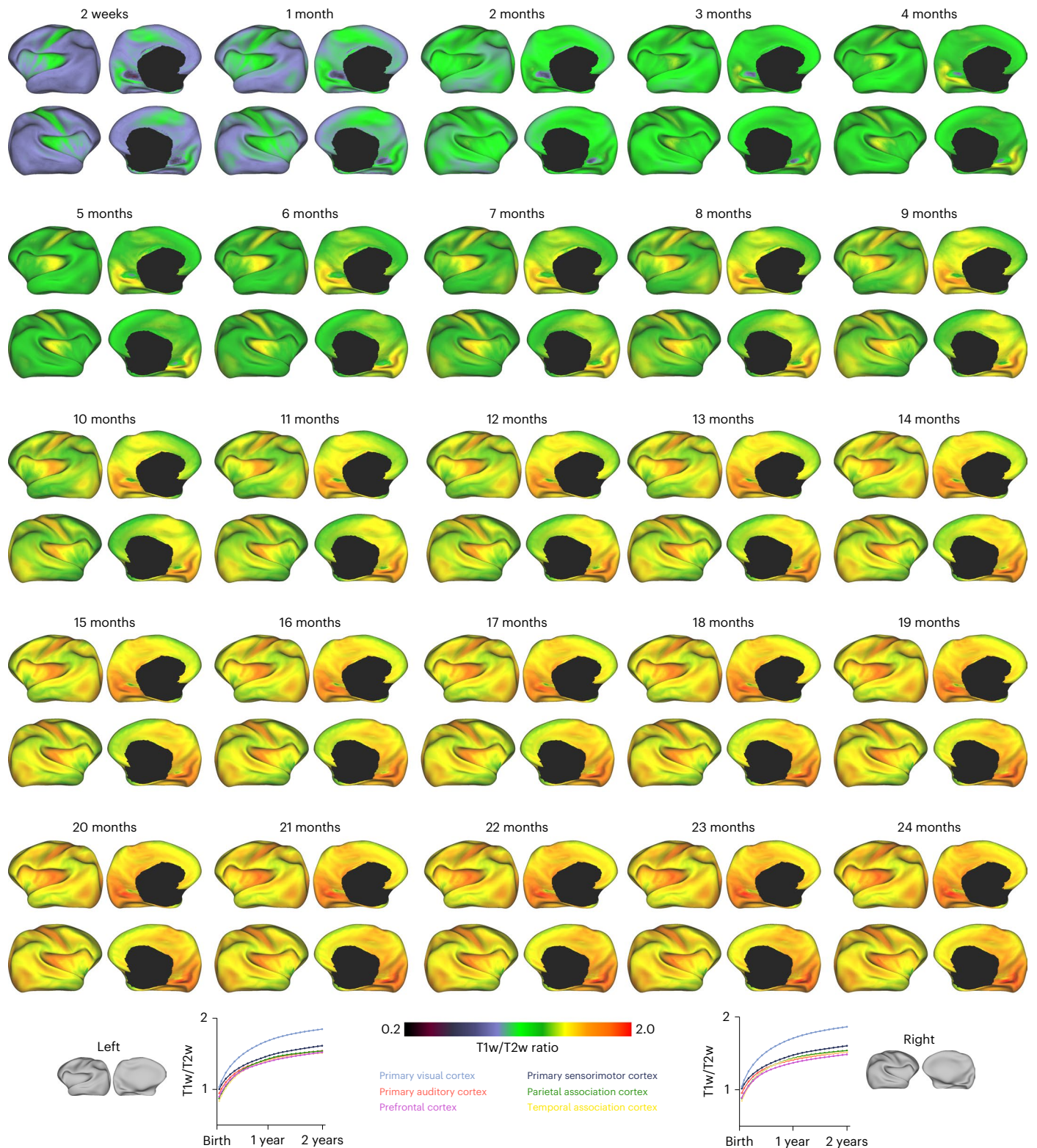
Fig. 6 | T1w/T2w ratio across infancy. Cortical T1w/T2w ratio, mapped onto the inflated white surfaces of the IBA.

of GM[37]. Axonal tracts accounting for WM form inter-hemispheric, cortico-cortical, limbic, brainstem, and cortico-spinal connections, providing an efficient network of structural connectivity[38,39]. Furthermore, CSF, apart from cushioning the brain, contributes to brain maturation and function by delivering growth factors and signaling molecules to progenitor cells that proliferate into immature neurons, which later migrate to different areas of the cerebral cortex[40,41]. IBA

growth curves for GM, WM, ventricular CSF, and whole-brain volume indicate that volumes of all tissues increase from birth through two years of age, albeit at rates different from previous studies. Knickmeyer et al.[4] reported changes in GM volume by 149% in the first year and 14% in the second year. More moderate changes were reported for the WM volume at 11% in the first year and 19% in the second year. On the other hand, the IBA increases in GM volume by 97.2% and 13.8%, and increase

in WM volume by 92.9% and 15.9%, during first and second postnatal years. These discrepancies can be due to differences in segmentation methods, percentage change definitions, and what were considered as WM and GM during volume calculation.

Overall, qualitative and quantitative analyses confirm that the surface–volume consistent IBA faithfully reflects the growth trajectories of infants with rich anatomical details. These atlases capture monthly changes in brain shape and size, cortical geometry, tissue contrast, volume, and microstructural characteristics of typically developing infants. A trait that sets the IBA apart from currently available atlases is that it covers each month during the first two postnatal years, providing a dense spatiotemporal depiction of this critical period of development. We hope that these atlases will become an invaluable common coordinate framework and facilitate the discovery of new insights into developmental processes underpinning child cognition and social behavior.

Online content

Any methods, additional references, Nature Portfolio reporting summaries, source data, extended data, supplementary information, acknowledgements, peer review information; details of author contributions and competing interests; and statements of data and code availability are available at https://doi.org/10.1038/s41592-022-01703-z.

References

1. Stiles, J. & Jernigan, T. L. The basics of brain development. *Neuropsychol. Rev.* **20**, 327–348 (2010).
2. Silbereis, J. C., Pochareddy, S., Zhu, Y., Li, M. & Sestan, N. The cellular and molecular landscapes of the developing human central nervous system. *Neuron* **89**, 248–268 (2016).
3. Gilmore, J. H., Knickmeyer, R. C. & Gao, W. Imaging structural and functional brain development in early childhood. *Nat. Rev. Neurosci.* **19**, 123–137 (2018).
4. Knickmeyer, R. C. et al. A structural MRI study of human brain development from birth to 2 years. *J. Neurosci.* **28**, 12176–12182 (2008).
5. Tanner, J. M., Whitehouse, R. H. & Takaishi, M. Standards from birth to maturity for height, weight, height velocity, and weight velocity: British children, 1965. i. *Arch. Dis. Child.* **41**, 454–471 (1966).
6. Bethlehem, R. et al. Brain charts for the human lifespan. *Nature* **604**, 525–533 (2022).
7. Margulies, D. S. et al. Situating the default-mode network along a principal gradient of macroscale cortical organization. *Proc. Natl Acad. Sci. USA* **113**, 12574–12579 (2016).
8. Oishi, K., Chang, L. & Huang, H. Baby brain atlases. *Neuroimage* **185**, 865–880 (2019).
9. Bozek, J. et al. Construction of a neonatal cortical surface atlas using multimodal surface matching in the developing human connectome project. *Neuroimage* **179**, 11–29 (2018).
10. Wu, Z. et al. 4D infant cortical surface atlas construction using spherical patch-based sparse representation. In *Medical Image Computing and Computer Assisted Intervention* (eds Descoteaux, M. et al.) 57–65 (HHS, 2017).
11. Oishi, K. et al. Multi-contrast human neonatal brain atlas: application to normal neonate development analysis. *Neuroimage* **56**, 8–20 (2011).
12. Shi, F. et al. Infant brain atlases from neonates to 1- and 2-year-olds. *PLoS ONE* **6**, 1–11 (2011).
13. Wang, L. et al. 4D multi-modality tissue segmentation of serial infant images. *PLoS ONE* **7**, 1–9 (2012).
14. Villalon, J., Joshi, A. A., Toga, A. W. & Thompson, P. Comparison of volumetric registration algorithms for tensor-based morphometry. In *IEEE International Symposium on Biomedical Imaging* 1536–1541 (IEEE, 2011).
15. Wu, J. et al. Accurate nonlinear mapping between MNI volumetric and FreeSurfer surface coordinate systems. *Hum. Brain Mapp.* **39**, 3793–3808 (2018).
16. Lecoeur, J. et al. Automated longitudinal registration of high resolution structural MRI brain sub-volumes in non-human primates. *J. Neurosci. Methods* **202**, 99–108 (2011).
17. Ahmad, S. et al. Surface–volume consistent construction of longitudinal atlases for the early developing brain. In *Medical Image Computing and Computer Assisted Intervention* (eds Shen, D. et al.) 815–822 (Springer, 2019).
18. Howell, B. R. et al. The UNC/UMN Baby Connectome Project (BCP): an overview of the study design and protocol development. *Neuroimage* **185**, 891–905 (2019).
19. Ahmad, S. et al. Surface-constrained volumetric registration for the early developing brain. *Med. Image Anal.* **58**, 101540 (2019).
20. Yeo, B. T. T. et al. Spherical demons: Fast diffeomorphic landmark-free surface registration. *IEEE Trans. Med. Imaging* **29**, 650–668 (2010).
21. Avants, B., Epstein, C., Grossman, M. & Gee, J. Symmetric diffeomorphic image registration with cross-correlation: evaluating automated labeling of elderly and neurodegenerative brain. *Med. Image Anal.* **12**, 26–41 (2008).
22. Severino, M. et al. Definitions and classification of malformations of cortical development: practical guidelines. *Brain* **143**, 2874–2894 (2020).
23. Fischl, B., Sereno, M. I. & Dale, A. M. Cortical surface-based analysis: II: Inflation, flattening, and a surface-based coordinate system. *Neuroimage* **9**, 195–207 (1999).
24. Lin, X. & Zhang, D. Inference in generalized additive mixed models by using smoothing splines. *J. Royal Stat. Soc. Series B Stat. Methodol.* **61**, 381–400 (1999).
25. Fischl, B. Freesurfer. *Neuroimage* **62**, 774–781 (2012).
26. Glasser, M. F. & Van Essen, D. C. Mapping human cortical areas in vivo based on myelin content as revealed by T1- and T2-weighted MRI. *J. Neurosci.* **31**, 11597–11616 (2011).
27. Johnson, M. H., Gliga, T., Jones, E. & Charman, T. Annual research review: Infant development, autism, and ADHD — early pathways to emerging disorders. *J. Child Psychol. Psychiat.* **56**, 228–247 (2015).
28. Hadders-Algra, M. Early diagnosis and early intervention in cerebral palsy. *Frontiers Neurol.* **5**, 185 (2014).
29. Langer, N. et al. White matter alterations in infants at risk for developmental dyslexia. *Cereb. Cortex* **27**, 1027–1036 (2015).
30. Yu, B. et al. HybraPD atlas: towards precise subcortical nuclei segmentation using multimodality medical images in patients with Parkinson disease. *Hum. Brain Mapp.* **42**, 4399–4421 (2021).
31. Wu, Z. et al. Construction of 4D infant cortical surface atlases with sharp folding patterns via spherical patch-based group-wise sparse representation. *Hum. Brain Mapp.* **40**, 3860–3880 (2019).
32. Girard, N., Raybaud, C., Gambarelli, D. & Figarella-Branger, D. Fetal brain MR imaging. *Magn. Reson. Imaging Clin. N. Am.* **9**, 19–56 (2001).
33. Valk, S. L. et al. Shaping brain structure: Genetic and phylogenetic axes of macroscale organization of cortical thickness. *Sci. Adv.* **6**, eabb3417 (2020).
34. Fjell, A. M. et al. Development and aging of cortical thickness correspond to genetic organization patterns. *Proc. Natl Acad. Sci. USA* **112**, 15462–15467 (2015).
35. Karama, S. et al. Childhood cognitive ability accounts for associations between cognitive ability and brain cortical thickness in old age. *Mol. Psych.* **19**, 555–559 (2014).
36. Wang, F. et al. Developmental topography of cortical thickness during infancy. *Proc. Natl Acad. Sci. USA* **116**, 15855–15860 (2019).
37. Purves, D. et al. *Neuroscience* (Oxford Univ. Press, 2017).
38. Yu, Q. et al. Differential white matter maturation from birth to 8 years of age. *Cereb. Cortex* **30**, 2674–2690 (2019).

39. Fields, R. D. Change in the brain's white matter. *Science* **330**, 768–769 (2010).
40. Shen, M. D. Cerebrospinal fluid and the early brain development of autism. *J. Neurodev. Dis*. **10**, 39 (2018).
41. Lehtinen, M. K. et al. The cerebrospinal fluid provides a proliferative niche for neural progenitor cells. *Neuron* **69**, 893–905 (2011).

Methods

Dataset and preprocessing

Longitudinal T1w and T2w MRI scans of 37 subjects (20 females and 17 males) enrolled as part of the UNC/UMN Baby Connectome Project (BCP)[18] were used in this work. Participants were recruited from existing registries at UNC and UMN based on state-wide birth records as well as from broader community resources (for example, community centers and targeted day-care centers) to ensure the sample approximates the racial/ethnic and socio-economic diversity of the US census. Informed consent was obtained from the parents of all subjects. The subjects were divided into six cohorts (A_1, A_2, A_3, B_1, B_2, and B_3) with first visits scheduled at 2 weeks, 1, 2, 9, 10, and 11 months, respectively. The subjects in A_1, A_2, and A_3 were scheduled to be scanned every 3 months in the first year and then at 24 months; whereas, the subjects in B_1, B_2, and B_3 were scanned every 3 months for the first 2 years. The total number of scans for each subject is different since not all subjects could be scanned at all expected time points. A total of 108 scans for each imaging modality were used. The study protocols were approved by the Institutional Review Board of the School of Medicine of The University of North Carolina at Chapel Hill.

The images were acquired using 3T Siemens Prisma MRI scanners equipped with Siemens 32-channel head coils. T1w MR images were acquired with 208 sagittal slices, TR/TE = 2,400/2.24 ms, flip angle = 8°, acquisition matrix = 320 × 320, and resolution = (0.8 mm)^3. T2w MR images were acquired with 208 sagittal slices, TR/TE = 3,200/564 ms, variable flip angles, acquisition matrix = 320 × 320, and resolution = (0.8 mm)^3.

MR images were quality-controlled using an automated algorithm[42] and then preprocessed using an infant-centric processing pipeline (iBEAT v.2.0; available at https://ibeat.wildapricot.org) consisting of the following steps:

(i) rigid alignment of T1w and T2w images using FLIRT[43];
(ii) skull stripping by a learning-based method[44];
(iii) intensity inhomogeneity correction by N3[45];
(iv) brain tissue segmentation by an infant dedicated learning-based method[46];
(v) hemisphere separation and subcortical filling; and
(vi) topologically-correct cortical surface reconstruction[47].

Example results of the processing steps are shown in Supplementary Fig. 15.

Surface–volume atlas construction

Our atlas construction method (Supplementary Fig. 16a) involves two main tasks:

(i) construction of the 12-month surface–volume atlas via surface-constrained groupwise registration; and
(ii) construction of longitudinal atlases for 2 weeks to 24 months by propagating the 12-month atlas through parallel transported longitudinal deformations.

The steps involved in each task are detailed below.

(i) Construction of reference atlas—IBA12. We first construct the 12-month surface–volume reference atlas, that is, IBA12, and use it to generate the atlases at the other time points. The IBA12 lies in the middle of the two-year time span and is hence ideal to capture developmental patterns between birth and two years of age.

Surface-constrained groupwise registration. The low intensity contrast of infant brain MRI renders image registration and atlas construction challenging. Here we use a dynamic elasticity model with surface constraint (SC-DEM[19]) for groupwise registration using tissue segmentation maps instead of intensity images. Groupwise registration allows a population of tissue segmentation maps to be registered

simultaneously to a common space as demonstrated in our previous work[17]. In our case, this is achieved by first selecting a reference based on a subject scan that is most similar in appearance to the whole set of images. Then, the reference tissue segmentation map is iteratively updated by fusing all tissue segmentation maps that are registered to it. SC-DEM improves the alignment of tissue boundaries using pre-determined surface transformations. Before SC-DEM groupwise registration, the tissue segmentation maps are affine-aligned with the reference tissue segmentation map using FLIRT[43]. From here on, affine transform is assumed to have taken place before SC-DEM registration unless otherwise stated.

For cortical surface registration, the white surface is inflated and mapped onto the unit sphere via metric distortion minimization[23]. The surfaces in the spherical space are represented by two folding attributes: average convexity and mean curvature. The spherical surfaces of the moving scans are registered to that of the reference scan using Spherical Demons[20]. The resulting vertex-wise correspondences are propagated to the white and pial cortical surfaces by leveraging the one-to-one vertex mapping between the spherical surfaces and the white and pial cortical surfaces.

SC-DEM employs a dynamic elasticity model[48] to characterize large nonlinear displacements. For the i-th subject scanned at time $\tau \in \mathcal{W}_{12}$ (in terms of chronological age), where $\mathcal{W}_\rho = [(\rho - 1.5), (\rho + 1.5)]$ months, we estimate displacement field with respect to a reference $\phi_{(i,\tau) \to \text{ref}}(\vec{x})$ by solving the wave equation:

$$\frac{\partial^2 \phi_{(i,\tau) \to \text{ref}}(\vec{x})}{\partial t^2} = \alpha \left(\nabla^2 \phi_{(i,\tau) \to \text{ref}}(\vec{x}) + \nabla \left(\nabla \cdot \phi_{(i,\tau) \to \text{ref}}(\vec{x}) \right) \right)$$
$$+ \beta f_{(i,\tau) \to \text{ref}}^{\text{vol}}(\vec{x}) + \gamma f_{(i,\tau) \to \text{ref}}^{\text{surf}}(\vec{x}), \tag{1}$$

where ∇^2 is the vector Laplacian operator and $f_{(i,\tau) \to \text{ref}}^{\text{vol}}(\vec{x})$ and $f_{(i,\tau) \to \text{ref}}^{\text{surf}}(\vec{x})$ are respectively the volumetric and surface force fields. The volumetric force field $f_{(i,\tau) \to \text{ref}}^{\text{vol}}(\vec{x})$ captures the misalignment between the warped moving tissue segmentation map $I_{(i,\tau)}(\vec{x} + \phi_{(i,\tau) \to \text{ref}}(\vec{x}))$ and the reference tissue segmentation map $I_{\text{ref}}(\vec{x})$:

$$f_{(i,\tau) \to \text{ref}}^{\text{vol}}(\vec{x}) = \left[I_{(i,\tau)}(\vec{x} + \phi_{(i,\tau) \to \text{ref}}(\vec{x})) - I_{\text{ref}}(\vec{x}) \right] \frac{\partial I_{(i,\tau)}(\vec{x} + \phi_{(i,\tau) \to \text{ref}}(\vec{x}))}{\partial(\vec{x} + \phi_{(i,\tau) \to \text{ref}}(\vec{x}))}. \tag{2}$$

The surface force field $f_{(i,\tau) \to \text{ref}}^{\text{surf}}(\vec{x})$ is computed on the basis of the differences between the volumetric displacements and the predetermined surface displacements for white and pial surfaces for both left and right hemispheres. The parameter α controls deformation smoothness and parameters β and γ balance the two force fields and control the rate of convergence. Registration halts when the two force fields are negligibly small, thereby consistently aligning the surface and the tissue segmentation map.

Cortical surface atlas. The cortical surface atlas comprising white and pial surfaces of both left and right hemispheres is constructed by using the registered cortical surfaces $\{\hat{S}_{(i,\tau)}\}_{(i,\tau)}$, each associated with a weight $w(\tau, 12)$, computed using $w(\tau_1, \tau_2) = \frac{1}{\sigma\sqrt{2\pi}} \exp\left(\frac{-(\tau_1 - \tau_2)^2}{2\sigma^2} \right)$, where parameter σ controls temporal smoothness and is set to 0.7 months. The 12-month cortical surface atlas A_{12}^{surf} is constructed by weighted averaging of the vertex coordinates for $\tau \in \mathcal{W}_{12}$: $\frac{\sum_{(i,\tau)} w(\tau,12)\hat{S}_{(i,\tau)}}{\sum_{(i,\tau)} w(\tau,12)}$. Next, we use A_{12}^{surf} to construct the corresponding volumetric atlas such that the two atlases are defined in the same coordinate space.

Volumetric atlas. The tissue segmentation volumetric atlas A_{12}^{tissue} is constructed by correcting the displacement fields $\{\phi_{(i,\tau)}(\vec{x})\}_{(i,\tau)}$ for $\tau \in \mathcal{W}_{12}$ on the basis of the surface atlas A_{12}^{surf}; ensuring the alignment of the volumetric WM–GM and GM–CSF interfaces in accordance with the surface atlas. This involves updating the volumetric displacement fields by considering surface misalignment as described below:

1. Compute for each vertex with coordinates $\vec{y}$ on the surface atlas the vertex-wise surface displacement $\Delta\psi_{(i,\tau)}(\vec{y})$ between $\hat{S}_{(i,\tau)}$ and A_{12}^{surf}.
2. Find in A_{12}^{surf} the triangle with vertices $\{\vec{y}_p\}_{p=1}^3$ closest to a query voxel $\vec{x}$.
3. Compute the corrective volumetric displacement field $\Delta\phi_{(i,\tau)}(\vec{x})$ as

$$\Delta\phi_{(i,\tau)}(\vec{x}) = \begin{cases} \frac{\sum_{p=1}^3 w(\vec{x},\vec{y}_p)\Delta\psi_{(i,\tau)}(\vec{y}_p)}{\sum_{p=1}^3 w(\vec{x},\vec{y}_p)} & \text{if } \parallel \vec{x} - \vec{y}_p \parallel \leq \delta, \quad \forall p; \\ 0 & \text{otherwise,} \end{cases} \tag{3}$$

where $w(\vec{x},\vec{y}) = \frac{1}{\sigma_g\sqrt{2\pi}}\exp\left(\frac{-\parallel\vec{x}-\vec{y}\parallel^2}{2\sigma_g^2}\right)$ and $\delta = 6$ mm. We set $\sigma_g = 3$ mm for smooth displacement fields.

4. Warp the tissue segmentation maps using the total displacement field $\phi_{(i,\tau)\to A_{12}^{\text{vol}}} = \phi_{(i,\tau)\to\text{ref}} + \Delta\phi_{(i,\tau)}$ for better alignment and preservation of anatomical details.
5. Determine the tissue label via majority voting for $\tau \in \mathcal{W}_{12}$.
6. Warp the intensity images (T1w and T2w) using the total displacement field $\phi_{(i,\tau)\to A_{12}^{\text{vol}}}$ to obtain $\{\hat{I}_{(i,\tau)}\}_{(i,\tau)}$.
7. Average the warped intensity images using the weights $\{w(\tau,12)\}$ to obtain 12-month T1w and T2w atlases: $A_{12}^{\text{int}} = \frac{\sum_{(i,\tau)}w(\tau,12)\hat{I}_{(i,\tau)}}{\sum_{(i,\tau)}w(\tau,12)}$.

(ii) Construction of longitudinal surface–volume atlases. The surface–volume atlases for 2 weeks to 24 months are generated by propagating the IBA12 to each month. To achieve this, we determine the average longitudinal change from each month to the 12-month atlas space. This is realized by transporting the longitudinal deformations to the atlas space via inter-subject deformations (Supplementary Fig. 16b).

Parallel transport of longitudinal deformations. The longitudinal growth of a subject is characterized by the displacement field $\phi_{(i,\tau')\to(i,\tau)}$ from time point τ' to time point $\tau \in \mathcal{W}_{12}$ estimated via affine and SC-DEM registration. Intra-subject deformation fields $\Phi_{(i,\tau')\to(i,\tau)} = \vec{x} + \phi_{(i,\tau')\to(i,\tau)}$ are spatially normalized to the 12-month atlas space by parallel transport[49]—disentangling inter-subject variability from longitudinal growth. The transported deformation field from the subject space to the 12-month atlas space is given as $\Phi^{\parallel}_{(i,\tau')\to(i,\tau)\to A_{12}^{\text{vol}}} = \Phi^{-1}_{(i,\tau)\to A_{12}^{\text{vol}}} \circ \Phi_{(i,\tau')\to(i,\tau)} \circ \Phi_{(i,\tau)\to A_{12}^{\text{vol}}}$.

Kernel regression. To construct age-specifc surface–volume consistent atlases, we warp the 12-month atlas to each specific time point τ_0 with the weighted average of the transported displacement fields $\{\phi^{\parallel}_{(i,\tau')\to(i,\tau)\to A_{12}^{\text{vol}}}\}_{\tau'\in\mathcal{W}_{\tau_0},\tau\in\mathcal{W}_{12}}$:

$$\phi^{\parallel}_{\tau_0\to A_{12}^{\text{vol}}} = \frac{\sum_i w(\tau',\tau_0)w(\tau,12)\,\phi^{\parallel}_{(i,\tau')\to(i,\tau)\to A_{12}^{\text{vol}}}}{\sum_i w(\tau',\tau_0)w(\tau,12)}. \tag{4}$$

The transported displacement fields are weighted based on whether τ' and τ are close to τ_0 and 12, respectively (Supplementary Fig. 16c). The displacement field $\phi^{\parallel}_{\tau_0\to A_{12}^{\text{vol}}}$ is used to warp the 12-month cortical surface and tissue segmentation maps atlases to each time point. Intensity images (T1w and T2w) are warped with total deformation fields $\Phi_{(i,\tau')\to(i,\tau)} \circ \Phi_{(i,\tau)\to A_{12}^{\text{vol}}} \circ \Phi^{\parallel -1}_{\tau_0\to A_{12}^{\text{vol}}}$ to obtain $\{\hat{I}_{(i,\tau')}\}_{(i,\tau')}$, which are averaged to generate T1w and T2w atlases: $A_{\tau_0}^{\text{int}} = \frac{\sum_i w(\tau',\tau_0)w(\tau,12)\,\hat{I}_{(i,\tau')}}{\sum_i w(\tau',\tau_0)w(\tau,12)}$.

Developmental trajectories of the infant population

To characterize infant brain maturation, we estimated the developmental trajectories of brain tissues volume, cortical thickness, surface area, average convexity, mean curvature, and cortical T1w/T2w ratio. For subject i at scan time t, the age effects on feature $f_i(t)$ are modeled using GAMM[24]: $f_i(t) = s(t) + \gamma_i$. Here, $s(\cdot)$ is a smooth nonlinear function represented by cubic regression splines and γ_i is the subject-specific random intercept. The degree of smoothness is selected using the restricted maximum likelihood criterion in R (https://www.r-project.org/).

Developmental trajectories of the IBA

To characterize developmental pattern captured by the IBA, we estimated the growth trajectories of surface and volumetric features. For the IBA at time point t, the age effects on feature $f(t)$ are modeled using the generalized additive model (GAM): $f(t) = s(t)$. Here, $s(\cdot)$ is a smooth nonlinear function represented by cubic regression splines. The degree of smoothness is selected using the restricted maximum likelihood criterion in R.

Statistical analysis for laterality

For each cortical ROI, we performed a one-sample two-tailed t-test at 1% significance level to determine whether the surface geometric features are significantly lateralized across the first two years of life.

Atlas construction with compared methods

For comparison purposes, we constructed (i) cortical surface atlases with Spherical Demons[20] and (ii) volume and surface atlases with ANTs[21]. We used developer-optimized parameters[20,50].

(i) Spherical Demons atlas construction. The cortical surface atlases at each month τ_0 are generated by groupwise registration of white surfaces of the subjects scanned at time $\tau' \in \mathcal{W}_{\tau_0}$. The white cortical surfaces are mapped onto the unit sphere and then spatially aligned via Spherical Demons, which uses average convexity and mean curvature to drive surface registration. During groupwise registration, individual cortical surfaces are aligned to the iteratively updated mean cortical surface. Finally, average convexity and mean curvature maps are averaged to obtain the surface atlases.

(ii) ANTs atlas construction. We first generate the 12-month surface and volume atlases, and use these to obtain atlases at the other time points. For the 12-month atlas, the tissue segmentation maps of the subjects scanned at time $\tau \in \mathcal{W}_{12}$ are spatially aligned via groupwise registration with ANTs. The cortical surfaces and intensity images of the registered subjects are then averaged with weights $\{w(\tau,12)\}$. The warped tissue segmentation maps are fused via majority voting. Next, we propagate these 12-month surface and volume atlases to each month τ_0 via parallel transport of intra-subject deformation fields estimated using affine and ANTs registration. Warped intensity images are weighted-averaged to obtain the T1w and T2w atlases.

Reporting summary

Further information on research design is available in the Nature Portfolio Reporting Summary linked to this article.

Data availability

Code availability

Software packages used for atlas construction include iBEAT v.2.0, Free-Surfer v.7.2, Spherical Demons v.1.4, FSL v.6.0.5, and RStudio v.1.2.1335. Additional code facilitating atlas construction is available under the MIT license via our project webpage (https://iba.yaplab.io).

References

42. Liu, S., Thung, K.-H., Lin, W., Yap, P.-T. & Shen, D. Real-time quality assessment of pediatric MRI via semi-supervised deep nonlocal residual neural networks. *IEEE Trans. Image Process.* **29**, 7697–7706 (2020).

43. Smith, S. M. et al. Advances in functional and structural MR image analysis and implementation as FSL. *Neuroimage* **23**, S208–S219 (2004).

44. Zhang, Q. et al. Frnet: flattened residual network for infant MRI skull stripping. In *2019 IEEE 16th International Symposium on Biomedical Imaging* 999–1002 (IEEE, 2019).

45. Sled, J. G., Zijdenbos, A. P. & Evans, A. C. A nonparametric method for automatic correction of intensity nonuniformity in MRI data. *IEEE Trans. Med. Imaging* **17**, 87–97 (1998).

46. Wang, L. et al. Volume-based analysis of 6-month-old infant brain MRI for autism biomarker identification and early diagnosis. In *Medical Image Computing and Computer Assisted Intervention* (eds Frangi, A. F. et al.) 411–419 (Springer, 2018).

47. Li, G. et al. Mapping region-specific longitudinal cortical surface expansion from birth to 2 years of age. *Cereb. Cortex* **23**, 2724–2733 (2013).

48. Ahmad, S. & Khan, M. F. Dynamic elasticity model for inter-subject non-rigid registration of 3D MRI brain scans. *Biomed. Signal Process. Control* **33**, 346–357 (2017).

49. Lorenzi, M. & Pennec, X. Efficient parallel transport of deformations in time series of images: from schild's to pole ladder. *J. Math. Imaging Vis.* **50**, 5–17 (2014).

50. Klein, A. et al. Evaluation of 14 nonlinear deformation algorithms applied to human brain MRI registration. *Neuroimage* **46**, 786–802 (2009).

Author contributions

S.A.: methodology, software, investigation, writing—original draft, writing—review and editing. Y.W.: writing—review and editing. Z.W.: data curation. K.-H.T.: data curation. S.L.: resources. W.L.: resources. G.L.: resources. L.W: resources. P.-T.Y.: conceptualization, supervision, funding acquisition, validation, writing—review and editing.

Competing interests

The authors declare no competing financial interests.

Additional information

Extended data is available for this paper at https://doi.org/10.1038/s41592-022-01703-z.

Supplementary information The online version contains supplementary material available at https://doi.org/10.1038/s41592-022-01703-z.

Correspondence and requests for materials should be addressed to Pew-Thian Yap.

Peer review information *Nature Methods* thanks Ulas Bagci, James Shine, and the other, anonymous, reviewer for their contribution to the peer review of this work. Primary Handling editor: Nina Vogt, in collaboration with the *Nature Methods* team.

Reprints and permissions information is available at www.nature.com/reprints.
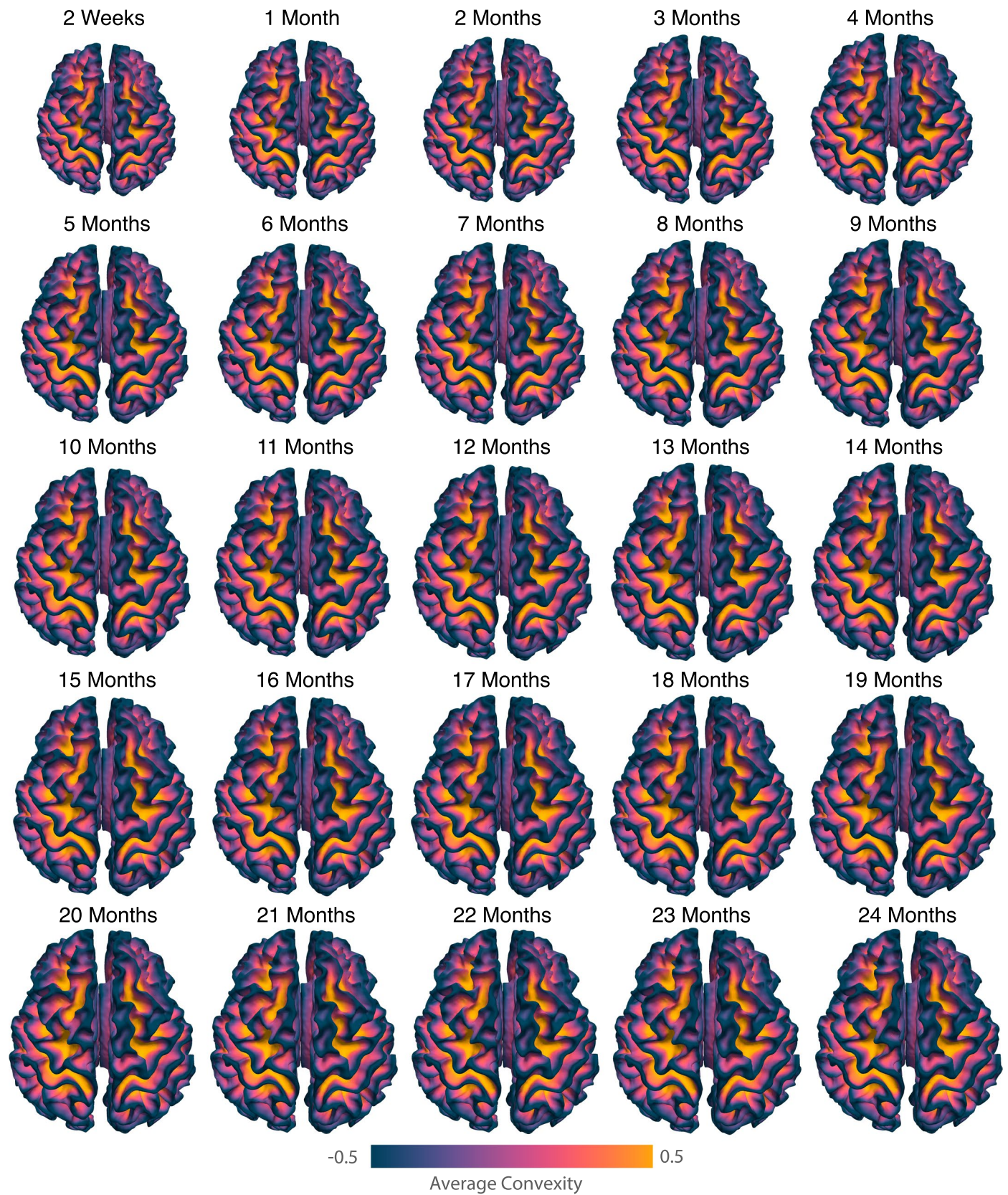
Extended Data Fig. 1 | Cortical atlases of the white surface. The age-specific cortical atlases of the white surface for both hemispheres, colored by average convexity (millimeter).
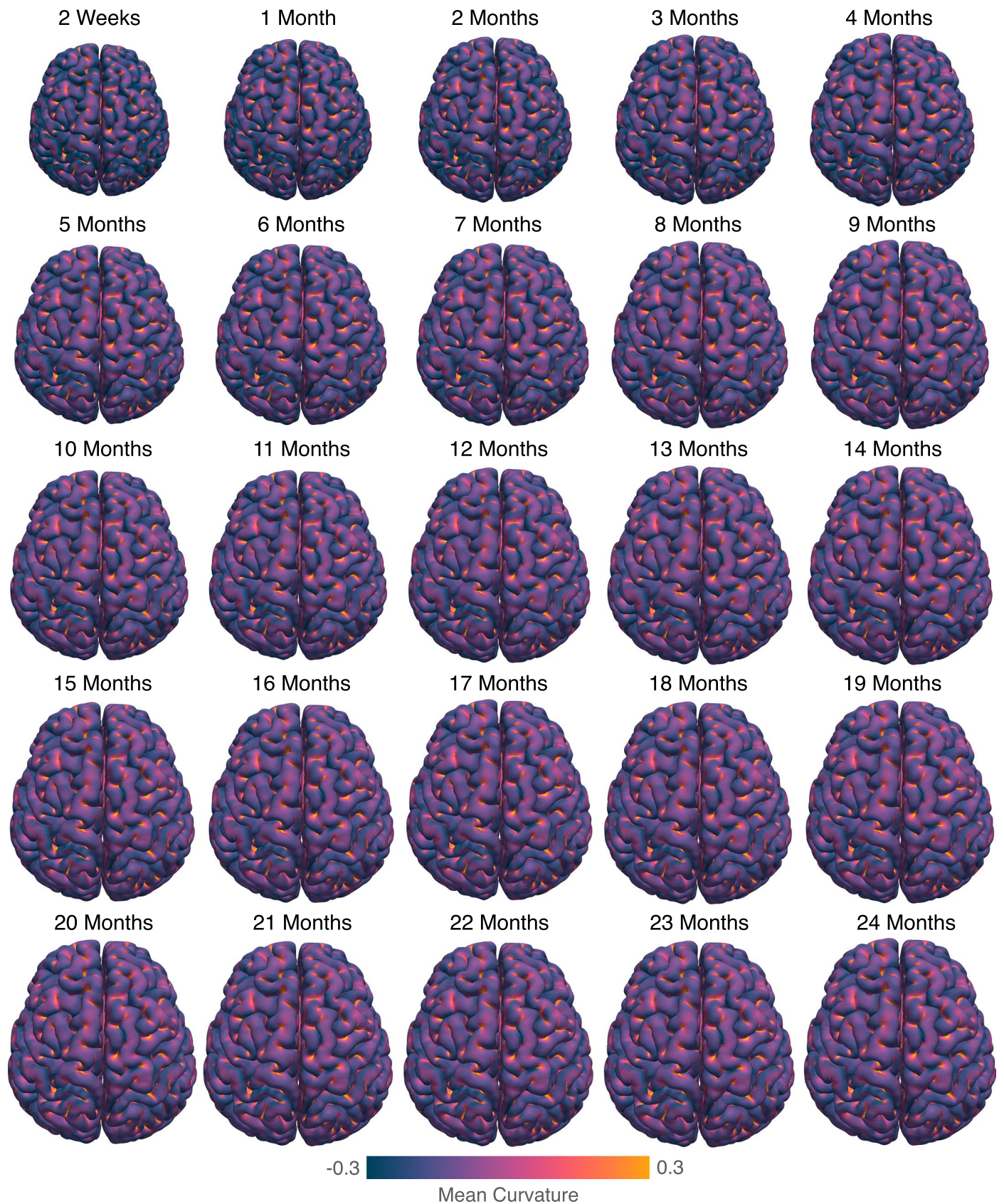
Extended Data Fig. 2 | Cortical atlases of the pial surface. Dorsal views of the age-specific cortical atlases of the pial surface for both hemispheres spanning 2 weeks to 24 months, colored by mean curvature (millimeter^{-1}).
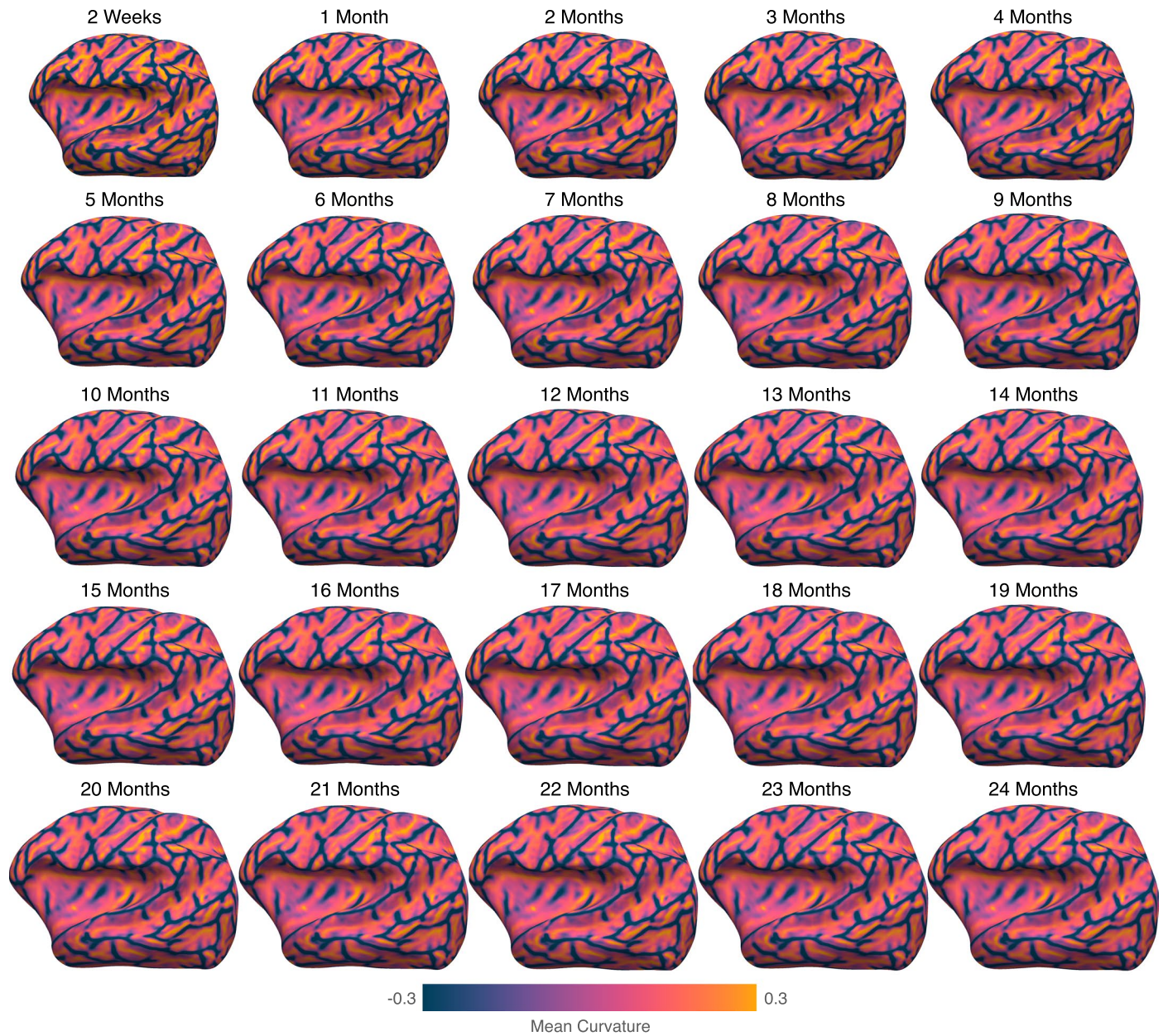
Extended Data Fig. 3 | Mean curvature maps of the longitudinal infant brain atlases. The inflated cortical atlases of the white surface (left hemisphere, lateral view) superimposed with mean curvature (millimeter^{-1}) spanning 2 weeks to 24 months.
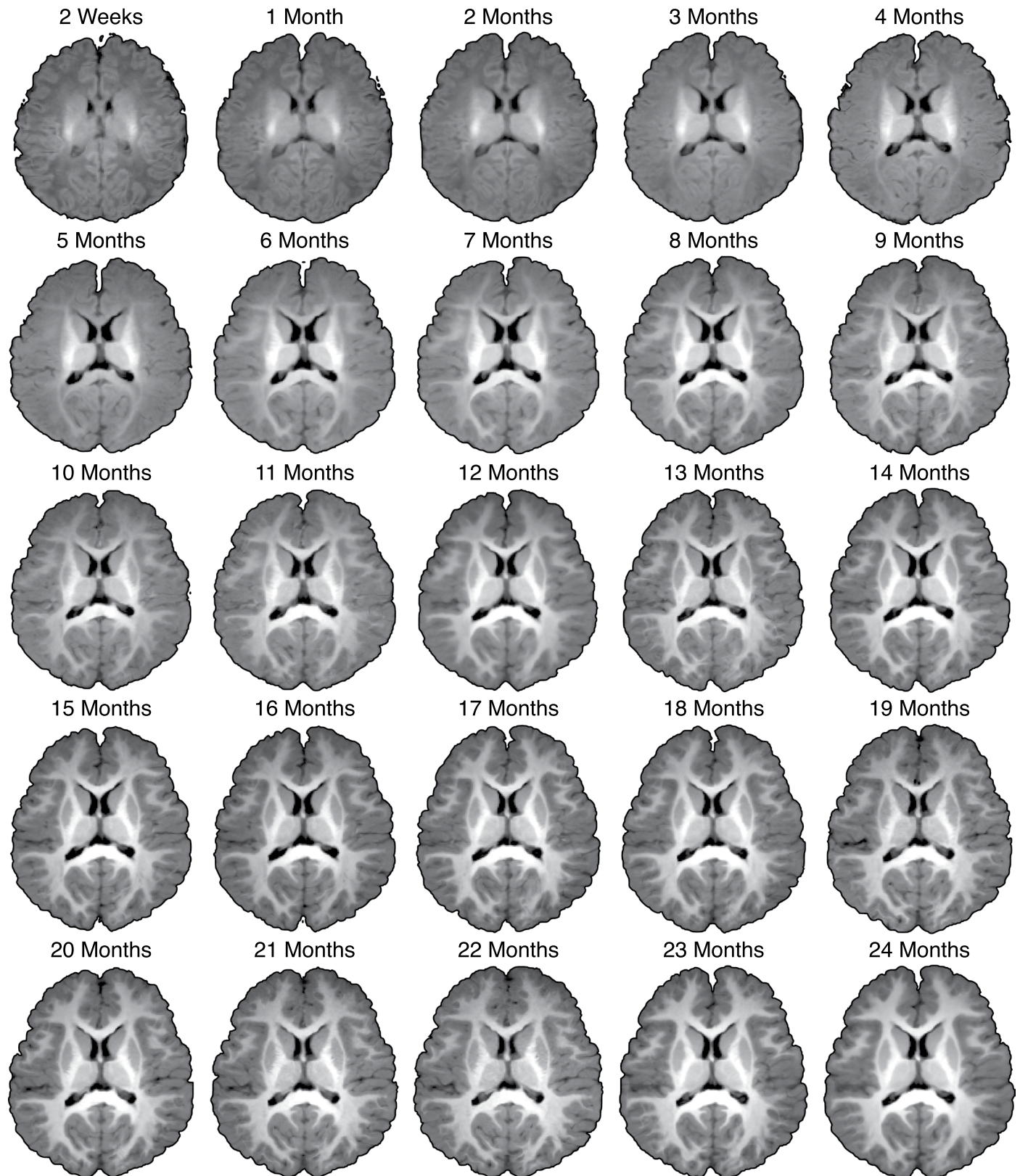
Extended Data Fig. 4 | T1w atlases of the infant brain. Transverse sections of the T1w atlases depicting dynamic changes in tissues contrast, size, and shape of anatomical structures at each month between 2 weeks and 24 months.
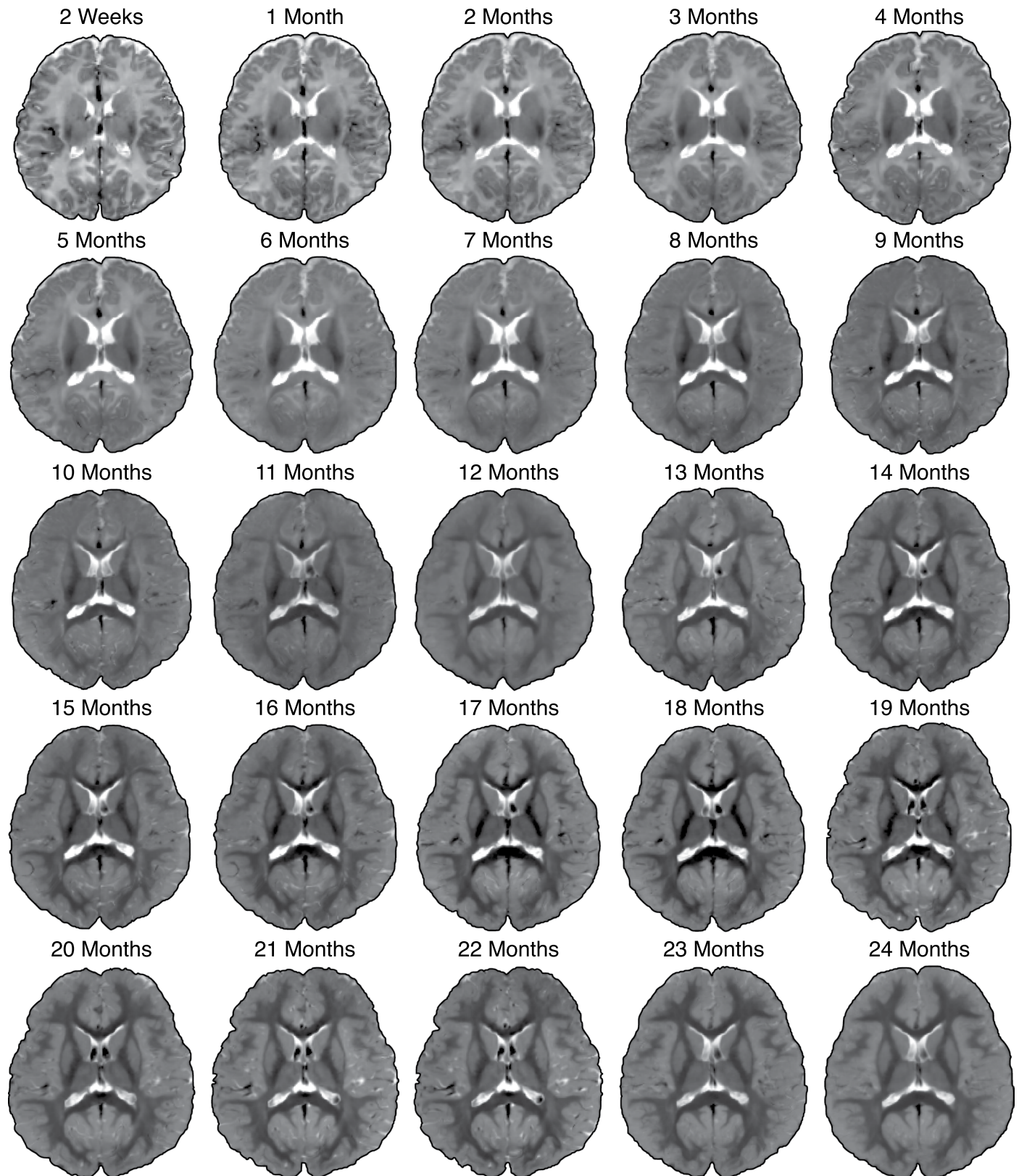
Extended Data Fig. 5 | T2w atlases of the infant brain. Transverse sections of the T2w atlases depicting dynamic changes in tissues contrast, size, and shape of anatomical structures at each month between 2 weeks and 24 months.
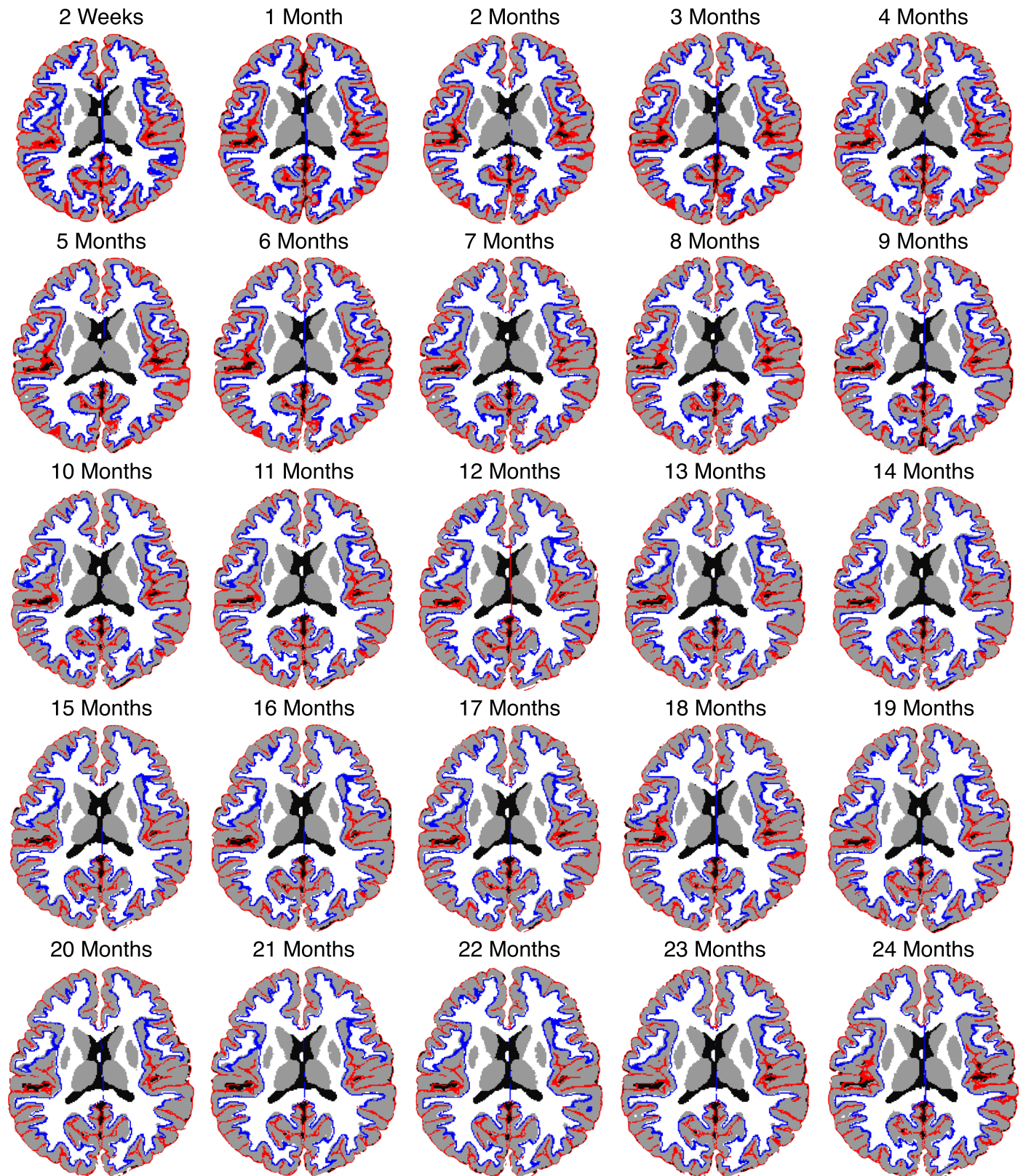
Extended Data Fig. 6 | Spatial consistency between age-specific cortical surface and volumetric atlases. Left and right cortical atlases of the white (*blue*) and pial (*red*) surfaces are superimposed onto the tissue segmentation atlases.
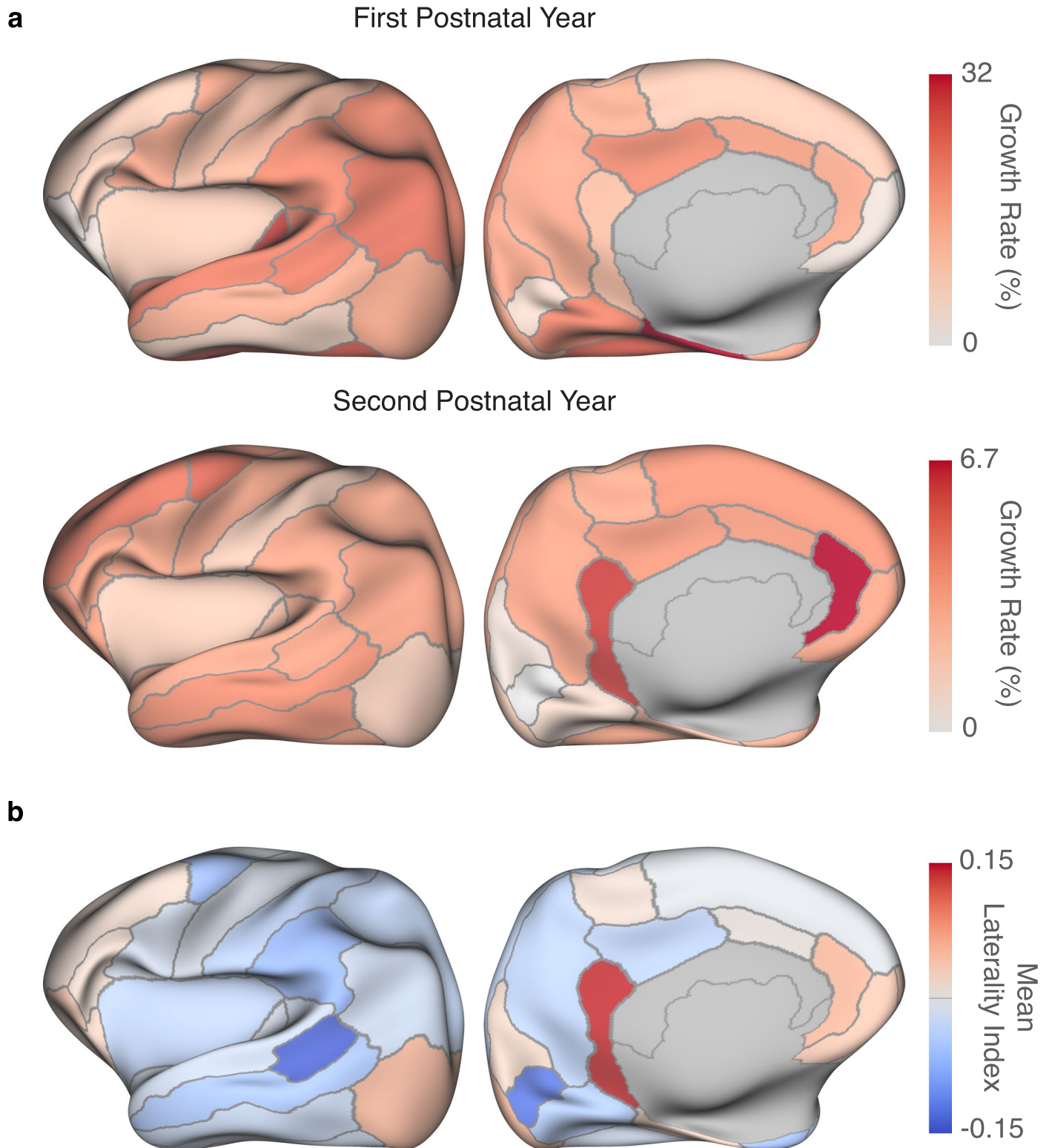
Extended Data Fig. 7 | Analysis of cortical thickness. a, Regional growth rates in terms of cortical thickness for the first (*top row*) and second (*bottom row*) postnatal years. **b**, ROI-specific mean laterality index for cortical thickness.

Extended Data Fig. 8 | Regional developmental trajectories of surface area. Growth curves of surface area for the IBA cortical regions. Shaded regions indicate whether surface area is higher or lower than the whole-brain average.

a

First Postnatal Year

Second Postnatal Year

b
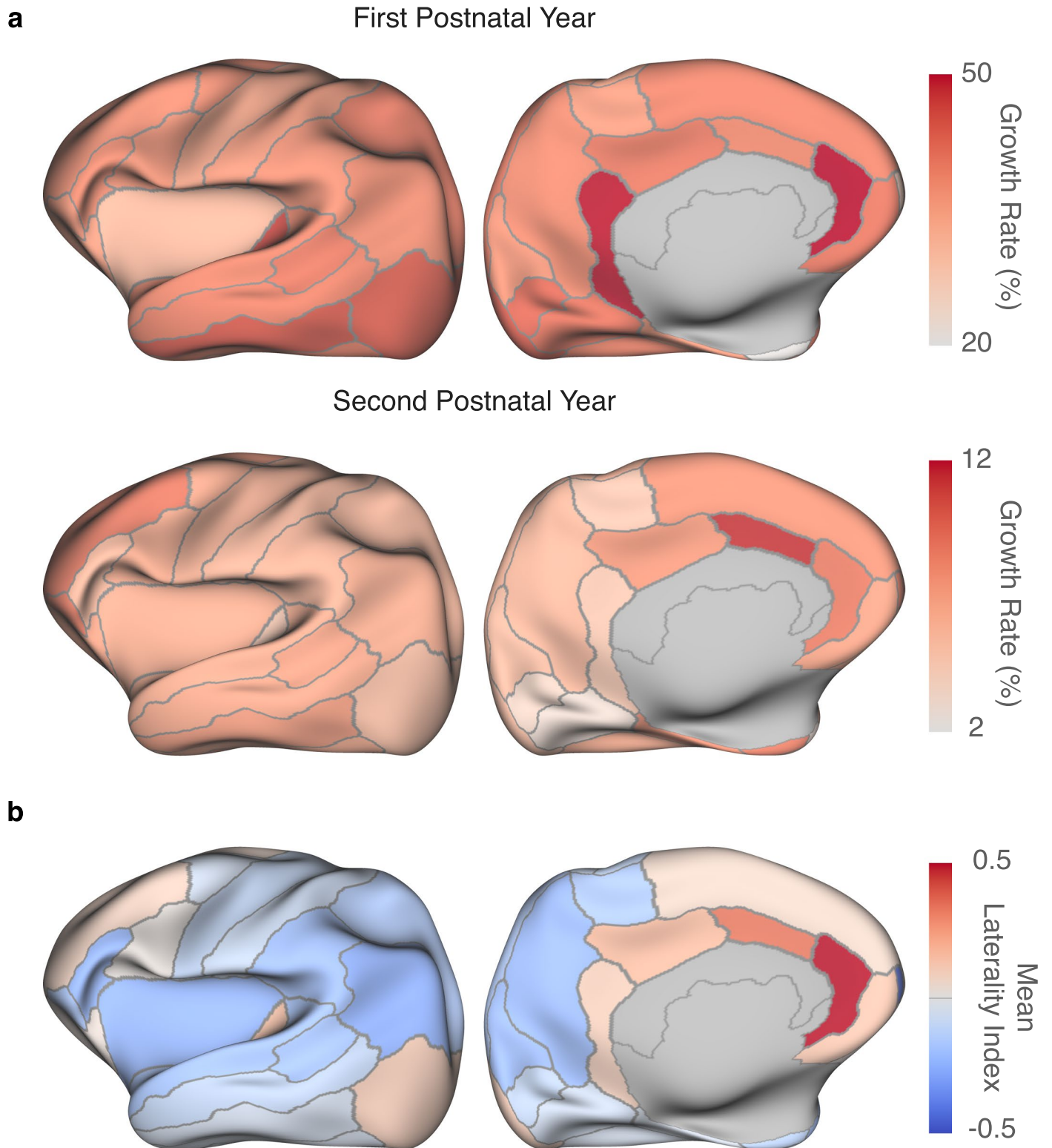
Extended Data Fig. 9 | Analysis of surface area. a, Regional growth rates in terms of surface area for the first (*top row*) and second (*bottom row*) postnatal years. **b**, ROI-specific mean laterality index for surface area.

Extended Data Fig. 10 | Hemispheric asymmetry of cortical thickness. Region-specific laterality index for cortical thickness of the IBA. Positive laterality is associated with left lateralization (two-tailed *t*-test: p < 0.01) and negative laterality is associated with right lateralization (two-tailed *t*-test: p < 0.01).

Corresponding author(s):   Pew-Thian Yap, Ph.D.

Last updated by author(s):   Oct 21, 2022

Reporting Summary

Nature Research wishes to improve the reproducibility of the work that we publish. This form provides structure for consistency and transparency in reporting. For further information on Nature Research policies, see our Editorial Policies and the Editorial Policy Checklist.

Statistics

For all statistical analyses, confirm that the following items are present in the figure legend, table legend, main text, or Methods section.

n/a	Confirmed	
☐	☒	The exact sample size (*n*) for each experimental group/condition, given as a discrete number and unit of measurement
☐	☒	A statement on whether measurements were taken from distinct samples or whether the same sample was measured repeatedly
☐	☒	The statistical test(s) used AND whether they are one- or two-sided *Only common tests should be described solely by name; describe more complex techniques in the Methods section.*
☒	☐	A description of all covariates tested
☒	☐	A description of any assumptions or corrections, such as tests of normality and adjustment for multiple comparisons
☐	☒	A full description of the statistical parameters including central tendency (e.g. means) or other basic estimates (e.g. regression coefficient) AND variation (e.g. standard deviation) or associated estimates of uncertainty (e.g. confidence intervals)
☐	☒	For null hypothesis testing, the test statistic (e.g. *F*, *t*, *r*) with confidence intervals, effect sizes, degrees of freedom and *P* value noted *Give P values as exact values whenever suitable.*
☒	☐	For Bayesian analysis, information on the choice of priors and Markov chain Monte Carlo settings
☒	☐	For hierarchical and complex designs, identification of the appropriate level for tests and full reporting of outcomes
☒	☐	Estimates of effect sizes (e.g. Cohen's *d*, Pearson's *r*), indicating how they were calculated

Our web collection on statistics for biologists contains articles on many of the points above.

Software and code

Policy information about availability of computer code

Data collection	No software was used
Data analysis	Atlas construction depends on several open-source software packages including: iBEAT v2.0, FreeSurfer v7.2, Spherical Demons v1.4, FSL v6.0.5, and RStudio v1.2.1335. Additional code facilitating atlas construction is available under the MIT license at our project webpage (https://iba.yaplab.io).

For manuscripts utilizing custom algorithms or software that are central to the research but not yet described in published literature, software must be made available to editors and reviewers. We strongly encourage code deposition in a community repository (e.g. GitHub). See the Nature Research guidelines for submitting code & software for further information.

Data

Policy information about availability of data

All manuscripts must include a data availability statement. This statement should provide the following information, where applicable:
- Accession codes, unique identifiers, or web links for publicly available datasets
- A list of figures that have associated raw data
- A description of any restrictions on data availability

The infant brain atlases are available at Zenodo (https://doi.org/10.5281/zenodo.7044932) under the Creative Commons Attribution Non Commercial Share Alike 4.0 International license.

The MRI data used in this work can be obtained from the National Institute of Mental Health Data Archive (NDA, https://nda.nih.gov/) or by contacting the investigative team. Source data for quantitative results in the main Figures 4, 5, and 6, Extended Data Figures 8 and 10, and Supplementary Figures 5, 7, 8, 10, 12, 13, and 17 are provided as Excel spreadsheets with this paper.

Field-specific reporting

Please select the one below that is the best fit for your research. If you are not sure, read the appropriate sections before making your selection.

☒ Life sciences   ☐ Behavioural & social sciences   ☐ Ecological, evolutionary & environmental sciences

For a reference copy of the document with all sections, see nature.com/documents/nr-reporting-summary-flat.pdf

Life sciences study design

All studies must disclose on these points even when the disclosure is negative.

Sample size	Longitudinal T1w and T2w MRI scans were acquired for 37 subjects (20 females; 17 males) enrolled as part of the UNC/UMN Baby Connectome Project (BCP). The subjects enrolled in the BCP study were divided into six cohorts (A1, A2, A3, B1, B2, B3), and each cohort's first visit was scheduled at 2 weeks, 1, 2, 9, 10, and 11 months, respectively. The subjects in A1, A2, and A3 were scheduled to be scanned every three months in the first year and then at 24 months; whereas, the subjects in B1, B2, and B3 were scanned every three months for the first two years. The total number of scans for each subject is different since all subjects cannot be scanned at all expected time points. A total of 108 scans for each imaging modality were used in the current work. Empirical results indicate that brain atlas variability decreases with sample size and reaches a subvoxel level with 30 samples (Supplementary Note 4). Thus, 108 longitudinal MRI scans from 37 subjects are sufficient for the purpose of this work.
Data exclusions	Data affected by artifacts, such as those caused by motion, were not included in our dataset.
Replication	We showed and discussed at length that our atlases reproduce findings observed in previous studies about brain development.
Randomization	Randomization is not applicable because this study does not involve comparison between groups.
Blinding	Blinding is not applicable because this study does not involve comparison between groups.

Reporting for specific materials, systems and methods

We require information from authors about some types of materials, experimental systems and methods used in many studies. Here, indicate whether each material, system or method listed is relevant to your study. If you are not sure if a list item applies to your research, read the appropriate section before selecting a response.

Materials & experimental systems

n/a	Involved in the study
☒	Antibodies
☒	Eukaryotic cell lines
☒	Palaeontology and archaeology
☒	Animals and other organisms
☐	☒ Human research participants
☒	Clinical data
☒	Dual use research of concern

Methods

n/a	Involved in the study
☒	ChIP-seq
☒	Flow cytometry
☐	☒ MRI-based neuroimaging

Human research participants

Policy information about studies involving human research participants

Population characteristics	Typically developing infants (51% female, 49% male), aged between birth and 5 years, were enrolled as part of the UNC/UMN Baby Connectome Project (BCP).
Recruitment	Participants were recruited from existing registries at UNC and UMN based on state-wide birth records as well as from broader community resources (e.g., community centers and targeted day-care centers) to ensure the sample approximates the racial/ethnic and socio-economic diversity of the US census.
Ethics oversight	The study protocols were approved by the Institutional Review Board of the School of Medicine of the University of North Carolina at Chapel Hill (UNC-CH), NC, USA.

Note that full information on the approval of the study protocol must also be provided in the manuscript.

Magnetic resonance imaging

Experimental design

Design type	Not applicable; only structural MRI, involving T1-weighted and T2-weighted images, was used.
Design specifications	Not applicable; only structural MRI, T1-weighted and T2-weighted images, was used.
Behavioral performance measures	Not applicable; only structural MRI, T1-weighted and T2-weighted images, was used.

Acquisition

Imaging type(s)	Structural T1-weighted and T2-weighted imaging.
Field strength	3T
Sequence & imaging parameters	MPRAGE, SPACE, FOV: 256mm x 256mm, slice thickness: 0.8mm.
Area of acquisition	Whole brain.
Diffusion MRI	☐ Used ☒ Not used

Preprocessing

Preprocessing software	iBEAT v2.0 (https://ibeat.wildapricot.org) for tissue segmentation maps and cortical surfaces.
Normalization	Data were normalized using rigid transform.
Normalization template	In-house brain template.
Noise and artifact removal	Bias-field correction.
Volume censoring	Not applicable. Only structural MRI, involving T1-weighted and T2-weighted images, was used. Images were quality-controlled before they were used.

Statistical modeling & inference

Model type and settings	Generalized additive mixture model (GAMM) and generalized additive model (GAM) with cubic regression, as described in the Methods section of the manuscript.
Effect(s) tested	Not applicable.
Specify type of analysis:	☒ Whole brain ☐ ROI-based ☐ Both
Statistic type for inference (See Eklund et al. 2016)	Models were fitted at the vertex level with goodness of fit determined via adjusted R^2.
Correction	Not applicable. Multiple comparisons not involved.

Models & analysis

n/a	Involved in the study
☒	☐ Functional and/or effective connectivity
☒	☐ Graph analysis
☒	☐ Multivariate modeling or predictive analysis